IN SITU STRUCTURAL CHARACTERIZATION OF FUNCTIONALLY GRADED NI-TI SHAPE MEMORY ALLOY DURING TENSILE LOADING

Francisco M. Braz Fernandes[1], Edgar Camacho[1], Patrícia F. Rodrigues[1], Patrick Inácio[2], Telmo G. Santos[2], Norbert Schell[3]

[1] CENIMAT/I3N, Department of Materials Science, FCT, Universidade NOVA de Lisboa, 2829-516 Caparica, Portugal

[2] UNIDEMI, Department of Mechanical and Industrial Engineering, NOVA School of Science and Technology, Universidade NOVA de Lisboa, 2829-516 Caparica, Portugal

[3] Institute of Materials Research, Helmholtz-Zentrum Geesthacht, Geesthacht, Germany

ABSTRACT

A functionally graded NiTi shape memory alloy wire was investigated by in-situ synchrotron radiation-based x-ray diffraction (SR-XRD) during cyclic tensile deformation. The transformation temperatures were determined by DSC and the thermomechanical behaviour was analysed by three-point bending test. The present study focussed on the localized heat treatment (Joule heat effect, reaching 300ºC, 350 and 400ºC pulses for 10 minutes) of NiTi wires, using an equipment that allows a large variety of graded conditions. Structural, mechanical and thermomechanical characterization is presented to get a perspective of the different types of graded functionality. A combination of two strategies has been used for the in situ analysis by SR-XRD of the tensile tests: (i) continuously following the structural evolution at one single point (at the center of the heat-treated segment) all long the load/unload cycle and (ii) scanning the full heat-treated segment at previously defined discrete steps of the stress-strain curve. The combined information from both types of tests provided detailed information about the phase transformations taking place in different regions of the functionally graded segment, at different steps of the tensile load/unload cycle, giving a better understanding of the overall mechanical, namely the evidence of the sequence B2 ↔ R ↔ B19' for the direct and reverse transformations.

KEYWORDS: Shape Memory Alloy; X-ray diffraction; Synchrotron; Functionally graded material.

ARTICLENOTE

This article is an invited submission to Shape Memory and Superelasticity selected from presentations at the 11th European Symposium on Martensitic Transformations (ESOMAT 2018) held August 27–31, 2018 in Metz, France, and has been expanded from the original presentation.

1. Introduction

NiTi alloys with shape memory effect and superelasticity have a wide range of engineering and biomedical applications due to their excellent mechanical properties [1].

These functional characteristics are a consequence of phase transformations that take place within well-defined temperature ranges or stress ranges, depending on being thermal or stress-induced. These temperature/stress ranges are a function of chemical composition and heat treatment of the material.

The precipitation reaction taking place during aging of Ni-Ti alloys may be used to finely adjust the composition of the Ni – Ti matrix and hence influence the transformation temperature of the heat-treated material. Under normal aging conditions (below 600ºC), only Ni_4Ti_3 precipitation is observed, which is the source of local stress fields that influence the nucleation and growth of R-phase and B19' martensite [2]. In addition, this precipitation is accompanied by a decrease in Ni content of the nearby NiTi matrix. Thus, Rs and Ms temperature will increase with aging time until finally reach a constant value that corresponds to the NiTi - Ni_4Ti_3 metastable-equilibrium composition at that temperature. This ''saturated'' transformation temperature after long time aging is dictated by the metastable equilibrium NiTi - Ni_4Ti_3 being thus only dependent on aging temperature and independent of alloy composition [1].

For applications requiring a wider controllable range, a wider temperature/stress range than that associated to a specific composition/heat treatment may be required.[3] In such a situation, the possible solution will

be to use a functionally graded material. Functional gradient may be introduced by: (i) a geometrical gradient (variable cross-section along a specific direction [4], (ii) a chemical composition gradient, either along the longitudinal direction [5], or along the thickness [3,6], (iii) a graded heat treatment [7], or (iv) may indirectly arise from a processing technique, such as laser welding [8].
Depending on the direction of the property or geometry gradient relative to the direction of loading, Shariat *et al.* [3] classified the designs into two types of gradient configuration: series and parallel designs. They also show that the series design may be well represented by the Maxwell (isostress) model in mechanics, in which the external load is applied in the direction of the gradient. The deformation (and the stress-induced transformation) will then occur sequentially and will extend from the higher heat treatment temperature region to the lowest one.
Shariat et al [5] used a temperature gradient field to anneal a cold worked NiTi wire, creating a functionally graded response along the length of the NiTi wire. These wires exhibited distinctive stress plateaus with positive slopes on strain. Increasing the temperature range of the gradient anneal increased the slopes of the stress plateaus associated with the stress-induced martensitic transformation.
Shariat et al. [3] and Meng et al. [7] reported that a Ni-Ti wire with 50.8% at. Ni (as-received sample), during the deformation, exhibits full pseudoelastic behaviour with a single stress-induced transformation plateau. But, after electrical heat treatment, two stress plateaus are shown:
(i) the deformation of the highest temperature heat-treated section of the wire displays a lower stress plateau and shows no recovery upon unloading,
(ii) the deformation of the unheated section of the wire displays the stress plateau value close to the as-received material and displays the pseudoelastic recovery upon unloading.
The localized heat treatment promoted the formation of the Ni_4Ti_3 precipitates; the internal section, being the one that was heated to a higher temperature, had a more intense precipitation which gave rise to a Ti-richer matrix; this higher Ti content of the matrix brings as a consequence a higher transformation temperature and, ultimately, also a lower critical stress for the austenite – martensite stress-induced transformation. [1]
In situ studies have been reported using neutrons [9] and synchrotron radiation [10,11,12,13,14,15] to provide very relevant information about the basic mechanisms of the stress-induced martensitic (SIM) transformation of NiTi (homogeneous) wires during superelastic regime.
It is the aim of the current work to present the characteristics of functionally graded NiTi shape memory wires, with localized heat treatment, in parallel with preliminary results of *in situ* SR-XRD. To achieve this purpose, two types of *in situ* cyclic loading/unloading tensile tests under synchrotron radiation were carried out: one where the structural evolution of the central point of the wire is followed and another one where the tensile test is interrupted at discrete points to scan the whole gauge length of the functionally graded wire. In this current study, the microstructurally graded Ni-Ti SMA produced by the local heat treatments may be well represented by the series configuration.

2. Materials and Methods

The material used for this study was 50.9 at% Ni - Ti wire (0.4 mm diameter) supplied by Euroflex.

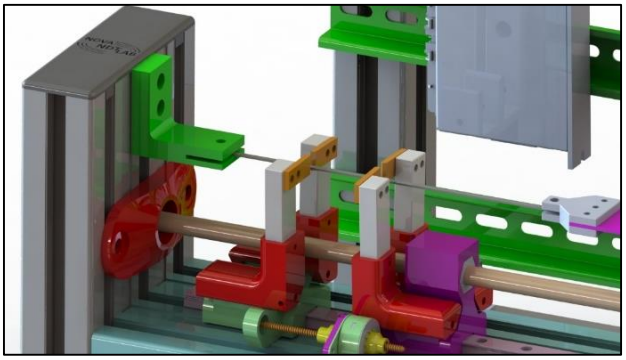

Figure 1 *–Schematic view of the home made electrical local heating system.*

A home-made equipment (Fig. 1) has been used to apply the localized heat treatments along the wires. A sliding contact system with two electrodes is used to inject an electrical current into the specimen. The segment between the two electrodes is heated by Joule effect. To impose an electrical current, a Keithley 2260-B DC power supply was used and can be programmed to set electrical current up to 70 A. To measure the temperature of the wire without disturbing the heat flow, an infrared camera Fluke Ti400 is used. Since the emissivity of the NiTi wire changes during heating and cooling cycle, it was applied a black coating for high temperature to keep the same emissivity (ε = 0.9) during the heat treatment. Thus, it was possible to perform a preliminary calibration to correlate the temperature with the electrical current imposed. The wires studied were heat-treated at 300 and 350 ºC for 10 and 30 min (Figure 2-a). 55-mm-length-samples were cut with and the localized heat treatment has been carried out along a 32-mm-long segment centered into the 55-mm-long wire (Figure 2-b). Inside this 32-mm-long-segment subjected to localized heat treatment, two segments of 8 mm length (hereafter referred to as external, where a greater temperature gradient exists) were separated from a central part 16 mm long (hereafter referred to as internal, where the temperature is practically uniform).

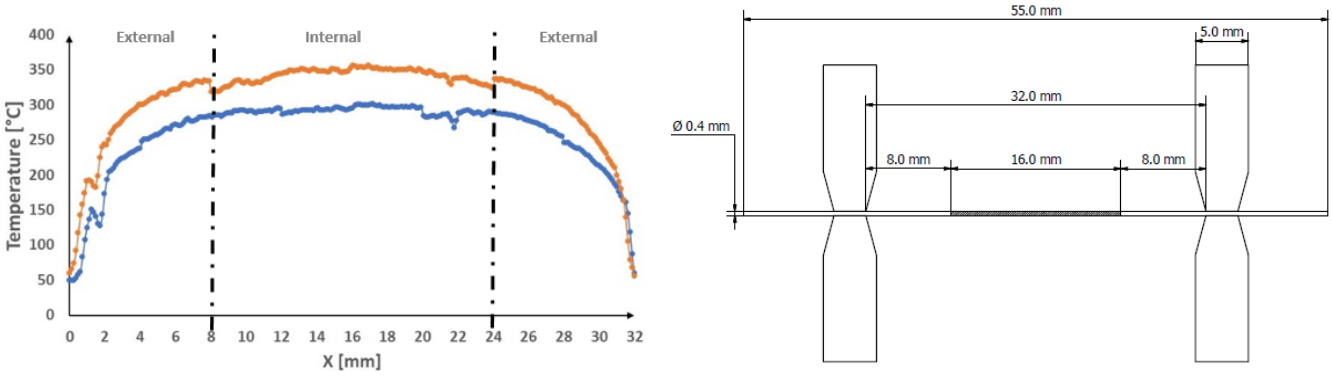

(a) (b)

***Figure 2** – Localized heat treatment of the NiTi wires:*

(a) Measured temperature profile for the heat treatments at 300 (blue curve) and 350 ºC (orange curve), at the central region.

(b) Subdivision of the wire in internal (16 mm long) and external segments (2 x 8 mm); see the text for details.

Transformation temperatures of the different segments of the heat-treated wires were determined by Differential Scanning Calorimetry (DSC) using a 204 F1 Phoenix from Netzsch. Two thermal cycles from -150 to +150 °C and -10 to 60 °C with heating/cooling rate of 10 K/min were used. This last DSC cycle was used to clarify the interpretation of TMA tests (run from -10 to 60 ºC). Before examination by DSC, the samples (~ 10 mg) were cut (from interior or exterior segments) and then chemically etched (10vol% HF + 45vol% HNO_3 + 45vol% H_2O) to remove the oxide, as well as the layer deformed by the cutting operation.

The tensile tests were performed in a Shimadzu NG50KN, using a 500 N load cell. All tests consisted of 3 cycles, run with a crosshead speed of 1 mm/min and maximum stroke of 6% of the gauge length. For each heat treatment condition, two different gauge lengths were tested:

(i) 32 mm gauge length, where the tensile test is representative of the total length of the localized heat treatment;

(ii) 44 mm gauge length, where the tensile test is representative of the “composite” behavior of the heat-treated segment (32 mm long) and two segments 6 mm long at each extremity that did not suffer the direct heating by Joule effect.

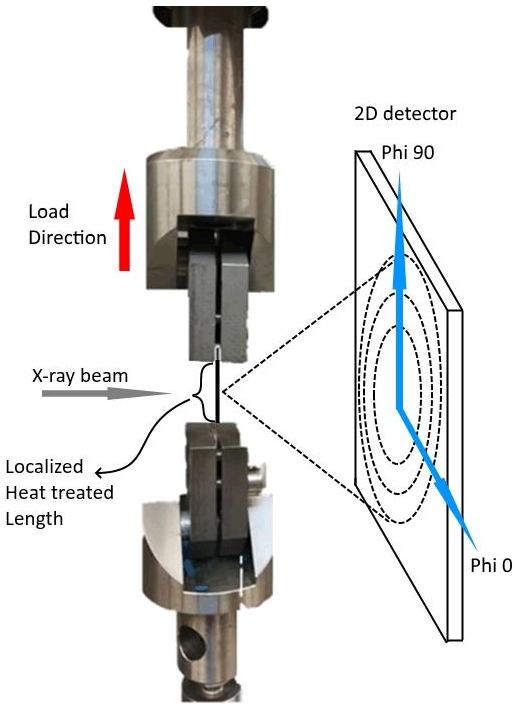

Figure 3 *– Schematic representation of the layout for the in situ XRD experiments during tensile tests. The relative positions of Phi=0º (horizontal) and Phi=90º (vertical) are also shown.*

The *in situ* tensile tests were performed in an INSTRON, test rig using a 20 kN load cell. Two types of tests were performed, up to 8% of the gauge length:

(i) complete load/unload cycle with discrete steps at previously fixed strain values where the full gauge length was scanned by the X-ray beam,

(ii) complete load/unload cycle where the X-ray beam was continuously hitting the central point of the gauge length.

In both cases a crosshead speed of 0.5 mm/min (~ .6 x 10^{-4} s^{-1}) has been used to guarantee that there was no temperature increase / decrease during load / unload.

The SR-XRD experiment on the localized heat-treated wire was performed in transmission mode, at beamline P07 High Energy Materials Science (HEMS) of PETRA III/DESY, using a wavelength of 0.124 Å (98 keV); a beam spot 500 × 200 μm^2 was used to scan the wire along its length and a 2D detector Perkin-Elmer was placed at 1.65 m from the sample. The raw 2D images were treated using Fit2D program to calculate the individual SR-XRD patterns:

- integration from 0 to 360º of each Debye-Scherrer ring; this is the case when no other specification is made;
- integration in 1º intervals to isolate specific azimuthal angles; in the current paper we have used only 0º, corresponding to the transversal direction on the wire, and 90º, corresponding to the longitudinal direction on the wire (Fig. 3).

The phases were identified according to ICDD-Standards.

3. Results and Discussion

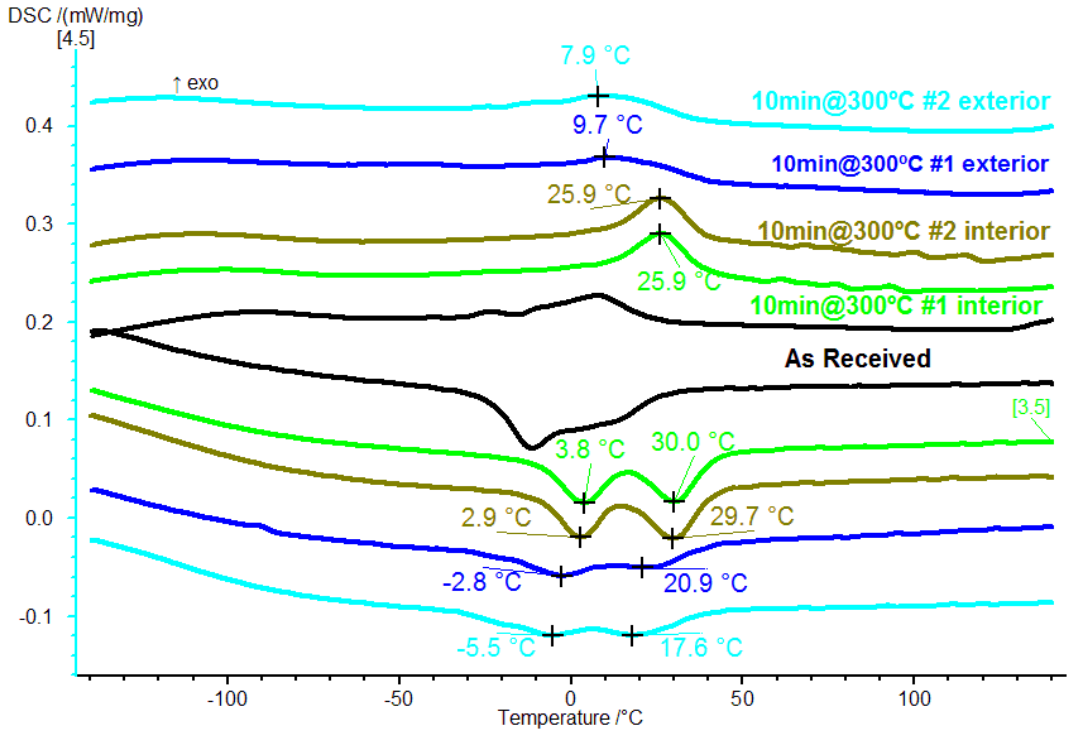

Figure 4 *– DSC results for the as-received wire and for 2 heat-treated wires (300 ºC for 10min).*

3.1Localized heat treatments

After the determination of the heating parameters to be used to obtain a maximum temperature of 300 ºC at the internal region of the Euroflex NiTi wires, these heating conditions have been used in consecutive trials, in different wires, to check the repeatability of the localized heat treatments. Fig. 4 shows the DSC results for:

- as-received wire,
- the internal segment of 2 wires with the same heat treatment at different occasions (2 weeks apart),
- the external segments of 2 wires with the same heat treatment at different occasions (2 weeks apart).

The very small differences between the two different heat-treated wires in terms of transformation temperatures and peak areas are negligible. These results allow us to state that the localized heat treatments may be considered reproducible with the equipment that has been used.

3.2Transformation temperatures as a function of heat treatment

The phase transformation temperatures of the as-received condition wire are represented in Table 1-(a) and the phase transformation temperatures of the internal and external segments of the heat-treated wire are presented in Table 1-(b) for the condition 300 ºC / 10 and 30 min and in Table 1-(c) for the condition 350 ºC / 10 and 30 min. They are designated by A, R and M, respectively for austenite (B2 structure), R-phase (trigonal structure), martensite (B19' structure) and the subscripts "s", "p" and "f", for start, peak and finish, respectively. M_f temperature is not listed because in the cases here studied the transformation to martensite on cooling was never finished at -150 ºC.

The analysis of this data shows that, for the cases here studied:

- for A → R, the transformation-start temperatures (Rs) of the heat-treated segments are always higher, compared to the as-received condition; the increasing transformation temperatures may be explained by the Ni_4Ti_3 precipitation [2];
- the transformations R →M (Ms) are kept constant for both segments of the 300 ºC / 10, 30 min condition compared to the as-received condition; a slight increase of Ms is identified for the condition 350 ºC, 10, 30 min that may be assigned to Ni enrichment following Ni_4Ti_3 precipitation;

- increasing aging duration from 10 to 30 min, increases the transformation temperatures for both aging temperatures (300 and 350 ºC); these results are in agreement with other authors reporting a significant increase of the transformation temperatures for short duration aging (below 1h); this increasing trend is followed by a stabilization for longer duration treatments;
- A_f temperatures for both heat-treated segments were always higher than for as-received wire; an increasing trend for the Af temperature has been reported by Huang et al for annealing temperatures up to 350 ºC [17].

Table 1. Transformation temperatures of the wires: as received (AR) material

Condition	Rs (°C)	Rp (°C)	Rf (°C)	Ms (°C)	As (°C)	Af (°C)
AR	27	6	-16	-63	-23	26

Table 2 Transformation temperatures of the wires: localized heat treatment at 300 °C, for 10 and 30 min

	Time (min)	Rs (°C)	Rp (°C)	Rf (°C)	Ms (°C)	As (°C)	Af (°C)
Int	10	39	27	12	-60	-8	42
	30	42	35	27	-60	-2	47
Ext	10	39	10	-17	-60	-35	42
	30	42	32	-25	-60	-35	47

Table 3 Transformation temperatures of the wires: localized heat treatment at 350 °C, for 10, 30 min

	Time (min)	Rs (°C)	Rp (°C)	Rf (°C)	Ms (°C)	As (°C)	Af (°C)
Int	10	30	23	5	-55	-11	34
	30	34	27	21	-41	-1	38
Ext	10	37	23	12	-43	-10	38
	30	40	31	25	-43	-5	44

3.3Mechanical characterization

The tensile tests on the wires at the different conditions (as-received and heat treated) are presented in Fig. 5.

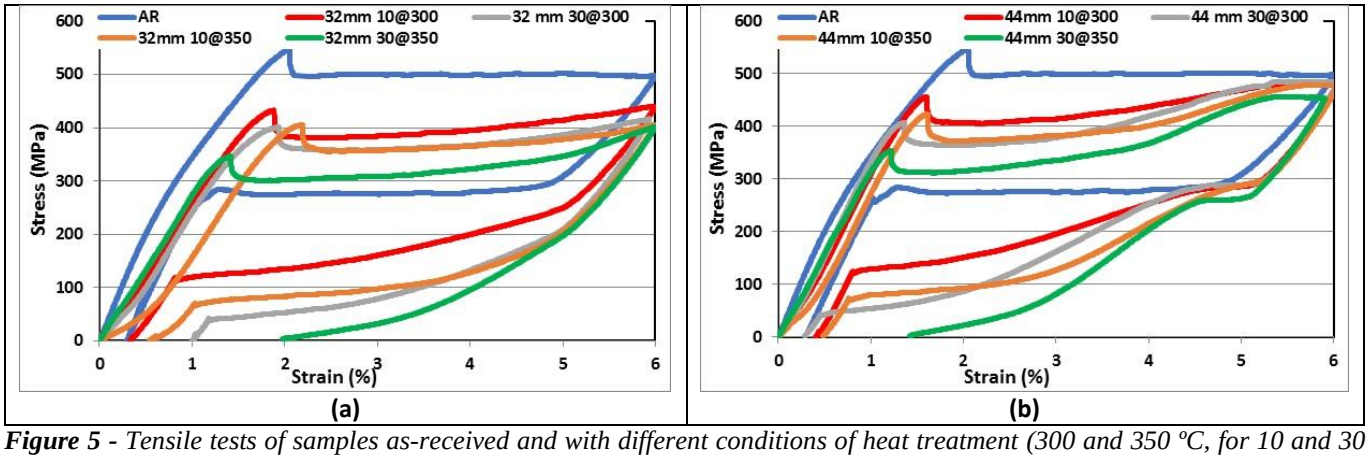

Figure 5 *- Tensile tests of samples as-received and with different conditions of heat treatment (300 and 350 ºC, for 10 and 30 min):(a) 32 mm gauge length and (b) 44 mm gauge length)*

For all wire conditions we observe:

(i) a two-step plateau, for the 44 mm gauge length,

(ii) a continuous increase of the slope of the "plateau", which is more notorious beyond ≈ 5 % strain, for the 32 mm gauge length.

For each heat treatment condition, the first step of the loading branch of the 44 mm gauge length is very close to that of the beginning of the plateau of the corresponding 32 mm gauge length. The second step of the loading branch of the 44 mm gauge length samples reached 450 to 500 MPa, very close to the stress level of the plateau for the as-received sample (475 to 500 MPa).

Comparing the stress values at 2.5 and 5.5% strains, which respectively represent the beginning and end part of the stress-induced-martensite (SIM) plateau, the stress increment is observed to range between 40 and 60 MPa for the 32 mm gauge length, while it ranges from 70 to 180 MPa for the 44 mm gauge length. These results are consistent with those found by other authors that report an increasing slope of the stress plateaus associated with the stress-induced martensitic transformation with increasing temperature range of the gradient anneal [5, 7]. It is apparent that the first plateau is associated with the central region (~16 mm) of the local heat-treated segment (32 mm), where the higher transformation temperatures give rise to lower critical stresses for the SIM transformation. For the 32 mm gauge length tests (Fig. 5-a) an increasing slope for the higher strains resulting from the graded structure produced by the steepest temperature gradient observed at the "external" regions is apparent (Figs. 2, 6), when compared to the flatter "internal" region. For the 44 mm gauge length, besides the lower stress plateau corresponding to the 32 mm heat-treated segment, a higher stress plateau is evident in association with the lower transformation temperatures (higher critical stress) of the two 6 mm long external segments (not directly heated by the Joule effect).

3.4 SR-XRD analysis

The *in situ* analysis results during the superelastic load/ unload cycle for two types of wires are presented: (i) wires where the heat-treated region (32 mm long) is used as gauge length during the tensile test and (ii) wires where a 44 mm gauge length has been used (32 mm heat-treated segment centered on the total gauge length).

A preliminary scan along the full gauge length was run before each tensile test. Austenite is present along the full gauge length (B2 110 peak), but along the central part of the localized heat-treated wire (32 mm long) R-phase is also present and, correspondingly, the $(110)_{B2}$ peak is slightly lower along this central region (Fig. 6). This figure illustrates that there is a good correspondence between the temperature profile registered during the localized heat treatment and the maximum intensity of the $(110)_{B2}$ peak. It is highlighted in the graph of Fig. 6 the fact that the maximum intensity of the $(110)_{B2}$ peak is reached in the wire external regions where the temperature during treatment is below 250 ºC. From our experience with this alloy, we know that no significant change of the transformation temperatures occurs for heat treatments below 250 ºC (with a duration up to 10 min as it is the case of the wires documented in Fig. 6). In addition, the lower values of the intensity of the (110)B2 for the 300 ºC / 10 min condition extend along a central region that is ~9 mm long (from 12 to 21 mm), while for the 350 ºC / 10 min condition it is ~23 mm long (from 4 to 27 mm).

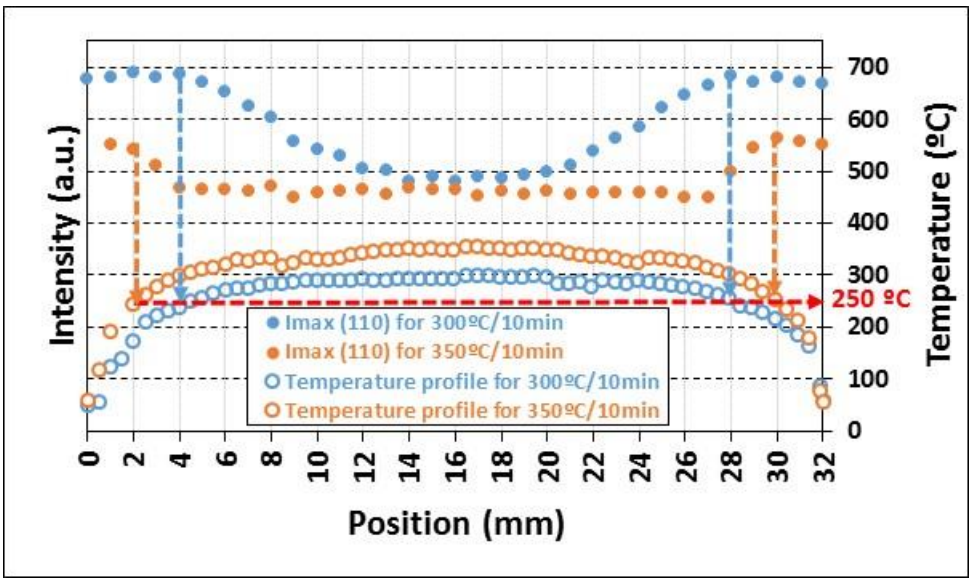

Fig. 6. *Comparison of the temperature profile during localized heat treatment at 300 and 350 ºC during 10 min and the maximum intensity of the (110) B2 peak along the heat-treated segment. The vertical dashed lines identify, for each heat treatment condition, the points along the wire where the (110)B2 intensity reached its maximum, starting from the central region of the segment. In both cases this corresponds to the points where the measured temperature was close to 250 ºC.*

The structural evolution has been followed with two different types of *in situ* tests:

(i) the X-ray beam always hitting the central point of the gauge length during the full load/unload cycle (Fig. 7) and

(ii) the full gauge length being scanned at previously defined arrest points of the stress-strain curve (Figs. 8 for the 44 mm gauge length and Fig. 9 for the 32 mm).

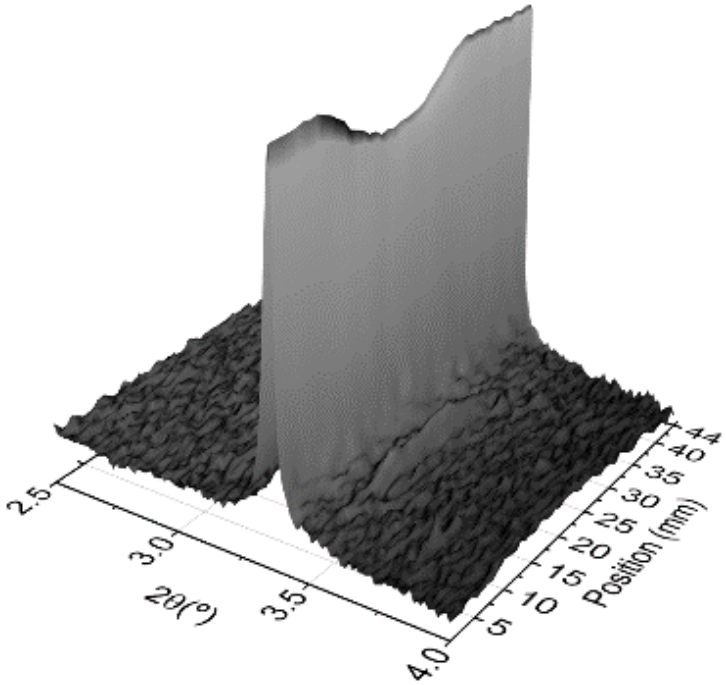

(a)

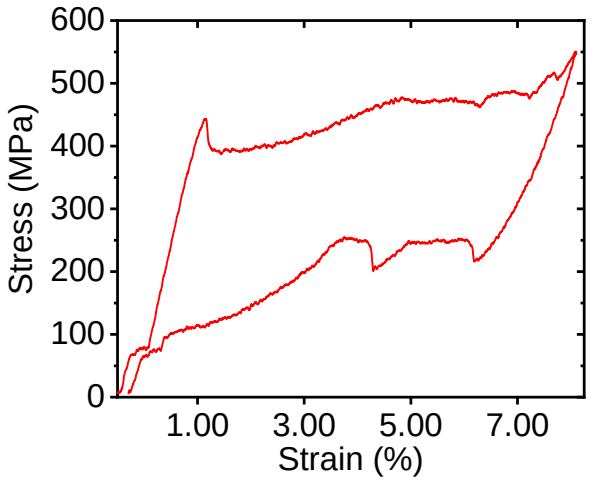

(b)

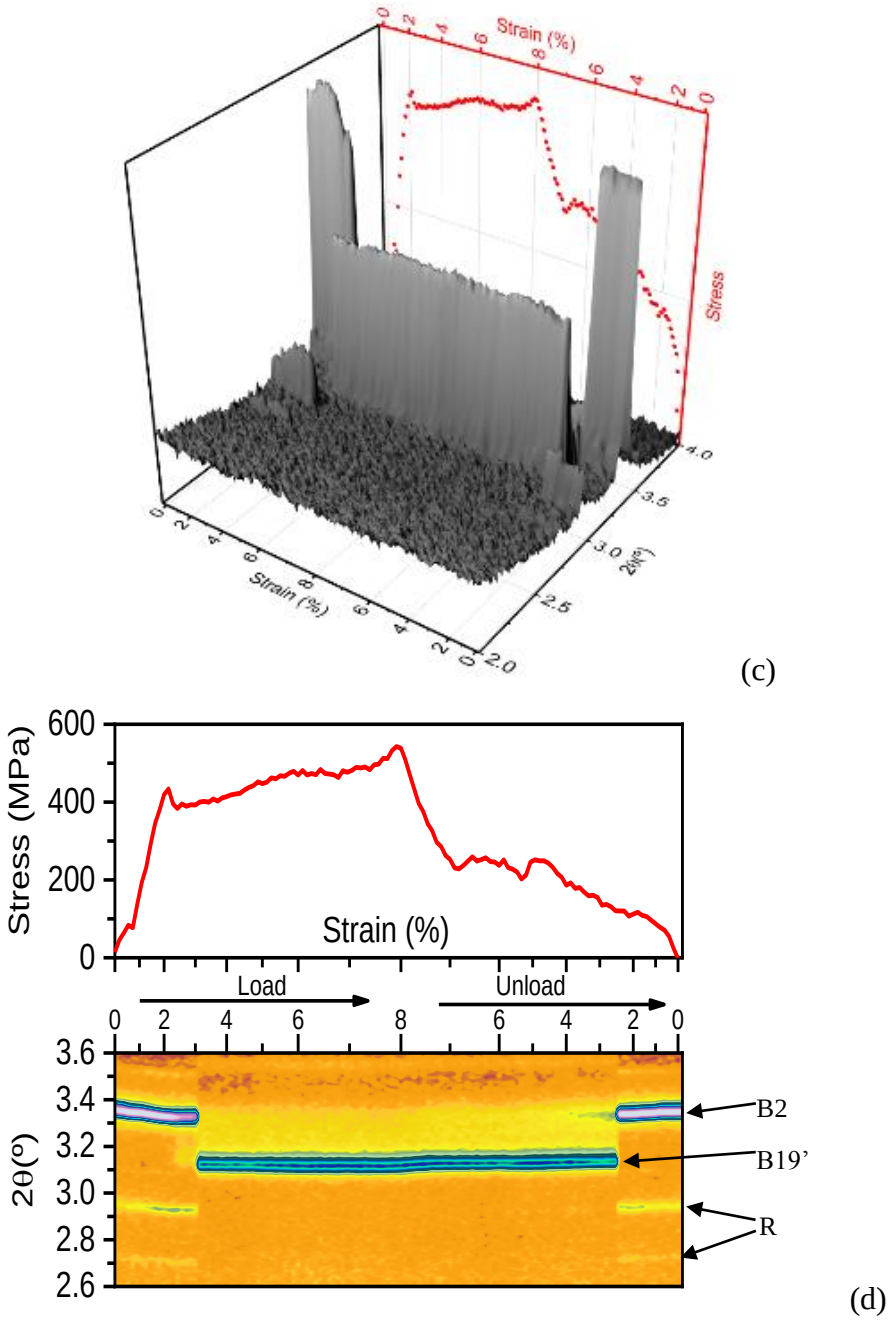

Fig. 7*. SR-XRD analysis of 44 mm long wire (local heat treatment at 300 ºC for 10 min of the 32 mm central part):*
(a) Initial profile of the heat-treated wire. Notice the higher intensity of the (110)B2 peak (Phi=90º) at the outermost segments (2 x 6 mm non heated by Joule effect) and the graded transition to the innermost 32 mm long segment (refer to Fig. 6).
(b) Stress strain curve of the superelastic regime registered during in situ SRXRD (beam always hitting the center of the wire).
(c) 3D plot of the scans (beam always hitting the center of the wire) during the load/unload.
(d) 2D contour plot of the scans (beam always hitting the center of the wire) during the load/unload.

Before running any mechanical test, the full gauge length of the wire (44 mm) has been scanned (Fig. 7-a). It puts in evidence the presence of both B2 and R-phase all long the wire, but with an increasing amount of R-phase approaching the central region and, correspondingly, a decreasing amount of B2. This feature is in agreement with the higher transformation temperatures of the internal segment of the wire.

The first type of *in situ* test provides a continuous identification of the structural changes that occur during the mechanical test, but only for the central point of the wire. With this type of test we can thus follow the structural changes induced at the point of the wire that has been subject to the highest temperature. An overall view of the stress-induced phase changes may be taken from Fig. 7-c), where we can identify the

more representative peaks of the austenite, R-phase and martensite. During loading, after a very short stabilization period (~0.5 % strain), the R-phase intensity starts increasing, while B2 intensity decreases; this corresponds to the stress-induced B2 → R also identifiable at the stress-strain curve. It is only at about 3 % strain (at the beginning of the stress-plateau, but significantly after the peak-stress at ~2% strain) that a sharp decrease of bot R and B2 peaks takes place. This sharp decrease of both peaks may be associated to a Lüders band nucleated very close to the central point of the wire, causing the appearance of B19'. During unloading, it is close to 2.5 % strain that B2 and R-phase peaks reappear (reverse transformation). In this last step it is noticed a slight decrease of the R-phase intensity, followed a stabilization up to final unloading. The sequence here found for these functionally graded wires (B2 → R → B19' on loading and the reverse order on unloading), in association with Lüders band mode of deformation is consistent with other authors results that are reported for homogeneous samples [18,19].

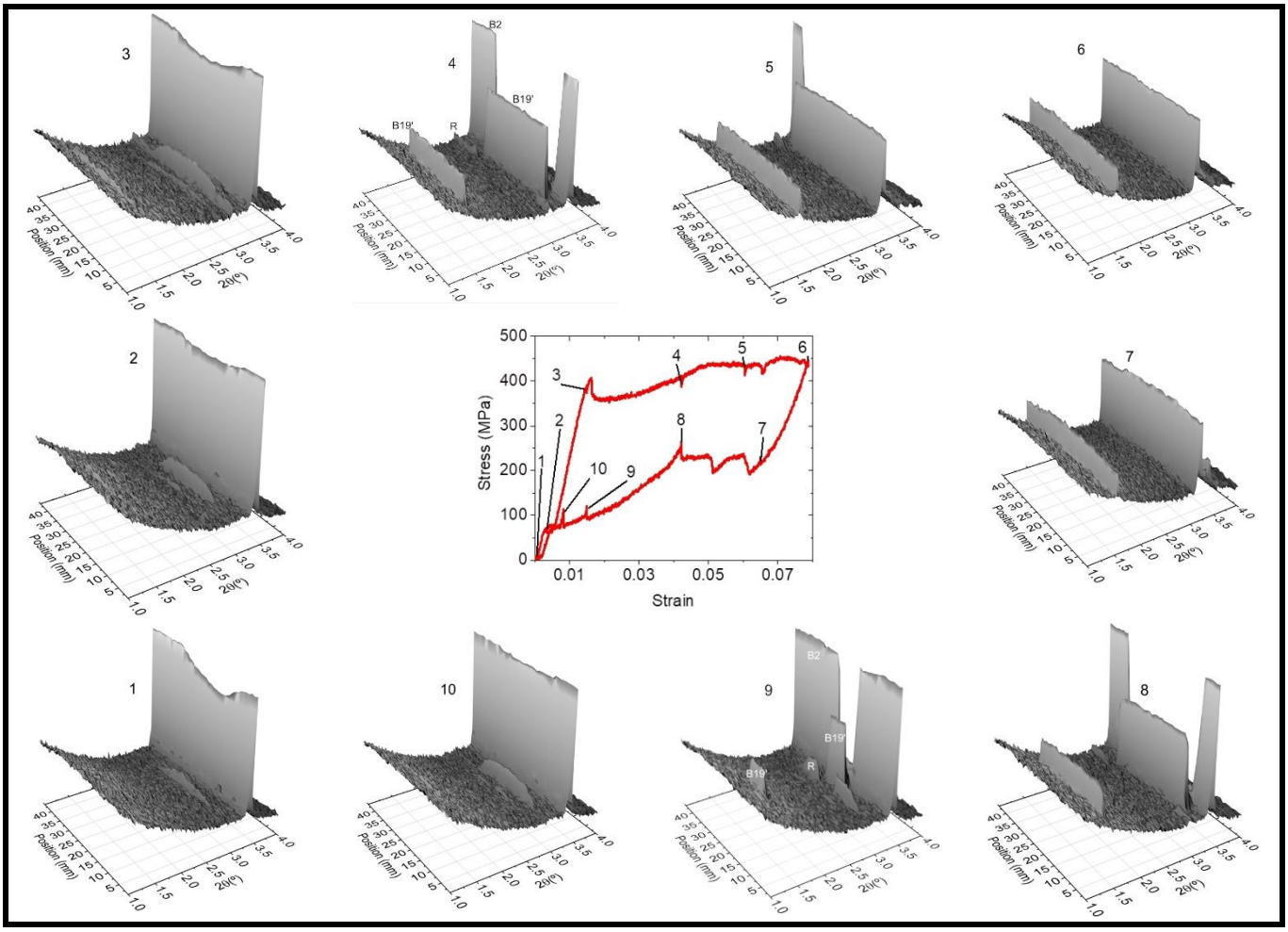

***Figure 8**– SR-XRD patterns (for Phi=90º) along the full gauge length (44 mm) of the heat-treated wire (local heat treatment at 300 ºC for 10 min of the 32 mm central part of the wire). The number at the top of each 3D scan identifies the position on the stress-strain curve. The identification of the more representative peaks of B2, B19' and R-phase is marked on the 3D patterns corresponding to the positions 4 and 9.*

Using the second type of *in situ* analysis (full scan of the gauge length at discrete steps of the mechanical test), we can see the structural changes that take place all long the wire at discrete steps of the tensile test, and correlate them with the Lüders band nucleation, its gradual progression and later regression.
On loading, the SIM is starting at the central region of the wire and, with gradually increasing stress, it progresses till it reaches both ends of the wire, both in the 44 mm and 32 mm gauge lengths. On the other hand, the reverse behavior can be observed during unloading: the reverse transformation progresses from

the edges to the central region of the wire. This results from the fact that the localized heat treatment promotes an overall increase of the transformation temperatures, which is more notorious at the central region of the wire, even for the 32-mm gauge length. During the unloading, the behavior is reversed, as expected. These observations show the existence of a functional gradient, even along the 32 mm locally heat-treated segment, as a result of the heat sink effect of the copper terminal contacts used for the Joule heating.

The *in situ* results identify the sequence B2 → R → B19' in both cases (gauge length 32 and 44 mm) for the 300 ºC / 10 min condition, illustrated in Figs. 8, 9, where the following structural details may be identified:

- R-phase intensity increases from position 1 to 2 (for both Figs 8, 9) and spreads gradually from the central regions to the extremities at position 3;
- at position 3, B19' starts to be formed (for both Figs 8, 9);
- at about 4% strain (point 4 for the 44 mm gauge length, Fig. 8; point 6 for the 32 mm gauge length, Fig. 9), the stress-induced B19' formation has extended to most of the central region of the wire for the 44 mm gauge length and R-phase still subsists at the extreme regions of both wires;
- at about 8% strain stress-induced B19' formation has extended to the full gauge length (point 6 for the 44 mm gauge length, Fig. 8; point 8 for the 32 mm gauge length, Fig. 9); at this last point, no R-phase is detected in both cases;
- during unloading, the reverse transformation takes place and R-phase starts to be formed (point 8 for the 44 mm gauge length, Fig. 8; point 10 for the 32 mm gauge length, Fig. 9);
- finally, after full unload, B19´ disappears and we have once again only B2 all along the gauge length and R-phase only in the central region.

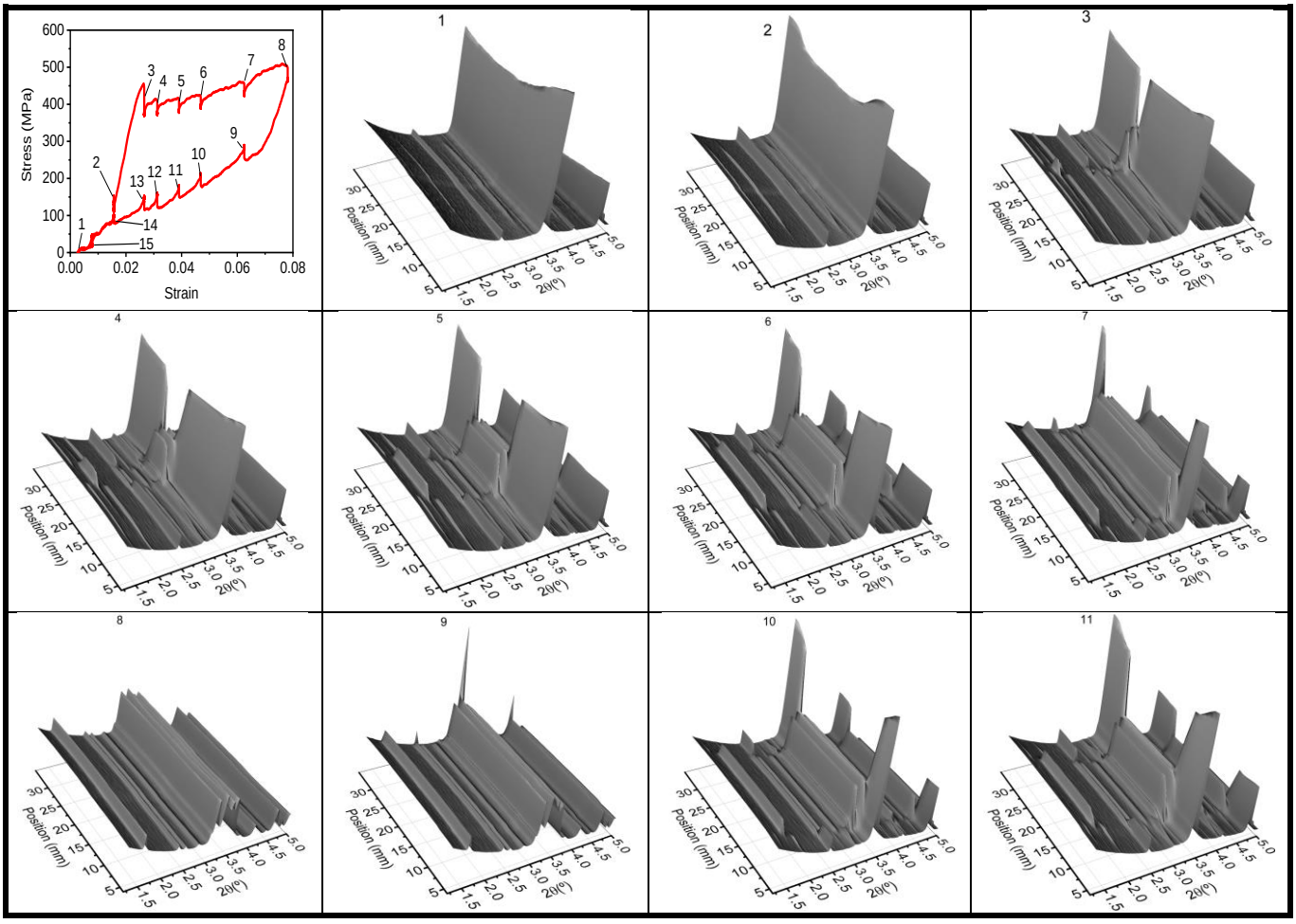

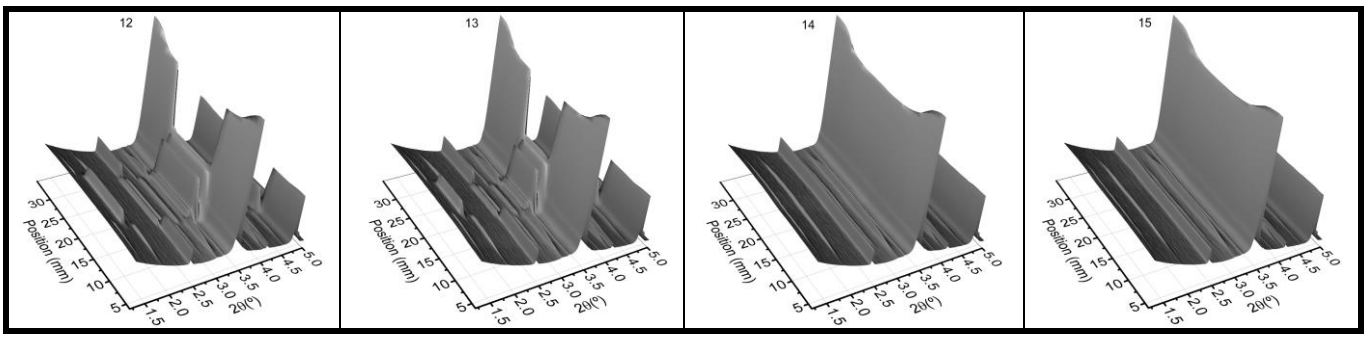

Figure 9 – *In situ SR-XRD analysis (for Phi=90º) during tensile test of the heat-treated wire (local heat treatment at 300 ºC for 10 min; gauge length comprising the 32 mm heat-treated region). The number at the top of each 3D scan identifies the position on the stress-strain curve.*

4. Conclusion

The following conclusions can be drawn:

- The functional gradient along the wire caused by the heat sink effect from the copper contacts used for the Joule heating has been put in evidence; such functional gradient may be used to get a "two-step" plateau for the SIM transformation;
- An overall increase of the transformation temperatures was obtained for heat treatments at 300 and 350 ºC for 10 and 30 min;
- The SIM transformation has been characterized by *in situ* SR-XRD analyses under load-unload tensile test, using two different experimental strategies: (i) in one case, a continuous follow-up of the central point of the wire, (ii) another type of test has been performing the full gauge length scan at previously chosen points where the stress-strain cycle was interrupted; the first option allows a more continuous follow-up of the structural evolution, but only for the central point; the second option gives a more detailed information about the structural evolution of different regions of the wire at discrete steps of the load/unload cycle;
- The intermediate R-phase is first stress-induced, followed by the B19' martensitic phase; for the cases studied here, both phase transformations had a very significant component of reversibility during load/unload.

Acknowledgements

Authors gratefully acknowledge the funding of Project POCI-01-0145-FEDER-016414 (FIBR3D), co-financed by Programa Operacional Competitividade e Internacionalização and Programa Operacional Regional de Lisboa, through Fundo Europeu de Desenvolvimento Regional (FEDER) and by National Funds through FCT - Fundação para a Ciência e a Tecnologia. P.F.R., EC and F.M.B.F acknowledge the funding of CENIMAT/I3N by National Funds through FCT - Portuguese Foundation for Science and Technology, Reference UID/CTM/50025/2019 and FCT/MCTES. P.F.R. acknowledges the funding of CAPES (CsF/ Brazil – BEX 11943-13-0). TS and PI acknowledge Fundação para a Ciência e a Tecnologia (FCT - MCTES) for its financial support of UNIDEMI via the project UID/EMS/00667/2019. Parts of this research were carried out at beamline P-07-HEMS at DESY, a member of the Helmholtz Association. The research leading to this result has been supported by the project CALIPSOplus under the Grant Agreement 730872 from the EU Framework Programme for Research and Innovation HORIZON 2020.

References

[1] Otsuka, K., Ren, X.: Physical metallurgy of Ti–Ni-based shape memory alloys. Prog. Mater. Sci. 50, 511–678 (2005).

[2] Shariat, B.S., Meng, Q., Mahmud, A.S., Wu Z., Bakhtiari, R., Zhang, J., Motazedian, F., Yang, H., Rio, G., Nam, T., Liu, Y.: Functionally graded shape memory alloys: design, fabrication and experimental evaluation. Materials and Design 124, 225–237 (2017).

[3] L. Bataillard, L., Bidaux, J.-E., R. Gotthardt, R: Interaction between microstructure and multiple-step transformation in binary NiTi alloys using in-situ transmission electron microscopy observations. Philosophical Magazine A, 78, 327-344 (1998).

[4] Shariat, B.S., Liu, Y., Rio, G.: Modelling and experimental investigation of geometrically graded NiTi shape memory alloys. Smart Mater. Struct. 22, 025030 (13 pp) (2013).

[5] Shariat, B.S., Liu, Y., Rio, G.: Thermomechanical modelling of microstructurally graded shape memory alloys. J Alloys Compd 541, 407–414 (2012).

[6] Martins, R.M.S. Schell, N., Gordo, P.R., Maneira M.J.P., Silva R.J.C., Braz Fernandes, F.M.: Development of sputtered Shape Memory Alloy (SMA) Ni–Ti films for actuation in ice cooled environments. Vacuum, 83, 1299-1302 (2009).

[7] Meng, Q., Wu, Z., Bakhtiari, R., Zhang, J., Yang, H., Liu, Y.: Stress serration and arch-shaped Lüders stress plateau behaviour of Ti–50.8at% Ni wire prepared by selective electrical resistance over-aging. Smart Mater. Struct. 25, 115035 (7 pp) (2016).

[8] Oliveira, J.P., Braz Fernandes, F.M., Miranda, R.M., Schell, N., Ocaña, J.L.: Effect of laser welding parameters on the austenite and martensite phase fractions of NiTi. Mater. Charact. 119, 148–151 (2016).

[9] Šittner, P., Lukáš, P., Novák, V., Daymond, M.R., Swallow, G.M.: In situ neutron diffraction studies of martensitic transformations in NiTi polycrystals under tension and compression stress. Materials Science and Engineering A 378, 97–104 (2004).

[10] Young, M.L., Wagner, M.F.-X., Frenzel, J., Schmahl, W.W., Eggeler, G.: Phase volume fractions and strain measurements in an ultrafine-grained NiTi shape-memory alloy during tensile loading. Acta Mater. 58, 2344–2354 (2010).

[11] Jones, N.G., Dye, D.: Martensite evolution in a NiTi shape memory alloy when thermal cycling under an applied load. Intermetallics 19, 1348–1358 (2011).

[12] Héraud, L., Castany, P., Lailllé, D., Gloriant, T.: In situ synchrotron X-ray diffraction of the martensitic transformation in superelastic Ti-27Nb and NiTi alloys: a comparative study. Materials Today: Proceedings 2S, S917 – S920 (2015).

[13] Sedmák, P., Pilch, J., Heller, L., Kopeček, J., Wright, J., Sedlák, P., Frost, M., Šittner, P.: Grain-resolved analysis of localized deformation in nickel-titanium wire under tensile load, Science 353, 559-562 (2016).

[14] Benafan, O., Garg, A., Noebe, R.D., Skorpenske, H.D., An, K., Schell, N.: Deformation characteristics of the intermetallic alloy 60NiTi. Intermetallics 82, 40-52 (2017).

[15] Hsu, W.N., Polatidis, E., Smíd, M., Casati, N., Van Petegem, S., Van Swygenhoven, H.: Load path change on superelastic NiTi alloys: In situ synchrotron XRD and SEM DIC. Acta Materialia 144, 874-883 (2018).

[17] Huang, X, Liu, Y.: Effect of annealing on the transformation behaviour and superelasticity of NiTi shape memory alloy. Scripta Materialia 45 153-160 (2001).

[18] Sittner, P., Sedlak, P., Landa, M., Novak, V., Lukas, P.: In situ experimental evidence on R-phase related deformation processes in activated NiTi wires Materials Science and Engineering A 438–440, 579–584 (2006).

[19] Héraud, L., Castany, P., Lailllé, D., Gloriant, T.: In situ synchrotron X-ray diffraction of the martensitic transformation in superelastic Ti-27Nb and NiTi alloys: a comparative study. International Conference on Martensitic Transformations, ICOMAT-2014. Materials Today: Proceedings 2S, S917 – S920 (2015).

Figure 1 – *Schematic view of the home made electrical local heating system.*

Figure 2 – *Localized heat treatment of the NiTi wires:*

(a) Measured temperature profile for the heat treatments at 300 (blue curve) and 350 ºC (orange curve), at the central region.

(b) Subdivision of the wire in internal (16 mm long) and external segments (2 x 8 mm); see the text for details.

Figure 3 – *Schematic representation of the layout for the in situ XRD experiments during tensile tests. The relative positions of Phi=0º (horizontal) and Phi=90º (vertical) are also shown.*

Figure 4 – *DSC results for the as-received wire and for 2 heat-treated wires (300 ºC for 10min).*

Figure 5 - *Tensile tests of samples as-received and with different conditions of heat treatment (300 and 350 ºC, for 10 and 30 min):(a) 32 mm gauge length and (b) 44 mm gauge length)*

Fig. 6. *Comparison of the temperature profile during localized heat treatment at 300 and 350 ºC during 10 min and the maximum intensity of the (110) B2 peak along the heat-treated segment. The vertical dashed lines identify, for each heat treatment condition, the points along the wire where the (110)B2 intensity reached its maximum, starting from the central region of the segment. In both cases this corresponds to the points where the measured temperature was close to 250 ºC.*

Fig. 7*. SR-XRD analysis of 44 mm long wire (local heat treatment at 300 ºC for 10 min of the 32 mm central part):*
(a) Initial profile of the heat-treated wire. Notice the higher intensity of the (110)B2 peak at the outermost segments (2 x 6 mm non heated by Joule effect) and the graded transition to the innermost 32 mm long segment (refer to Fig. 6).
(b) Stress strain curve of the superelastic regime registered during in situ SRXRD (beam always hitting the center of the wire).
(c) 3D plot of the scans (beam always hitting the center of the wire) during the load/unload.
(d) 2D contour plot of the scans (beam always hitting the center of the wire) during the load/unload.

Figure 8– *SR-XRD patterns (for Phi=90º) along the full gauge length (44 mm) of the heat-treated wire (local heat treatment at 300 ºC for 10 min of the 32 mm central part of the wire). The number at the top of each 3D scan identifies the position on the stress-strain curve. The identification of the more representative peaks of B2, B19' and R-phase is marked on the 3D patterns corresponding to the positions 4 and 9.*

Figure 9 – *In situ SR-XRD analysis (for Phi=90º) during tensile test of the heat-treated wire (local heat treatment at 300 ºC for 10 min; gauge length comprising the 32 mm heat-treated region). The number at the top of each 3D scan identifies the position on the stress-strain curve.*

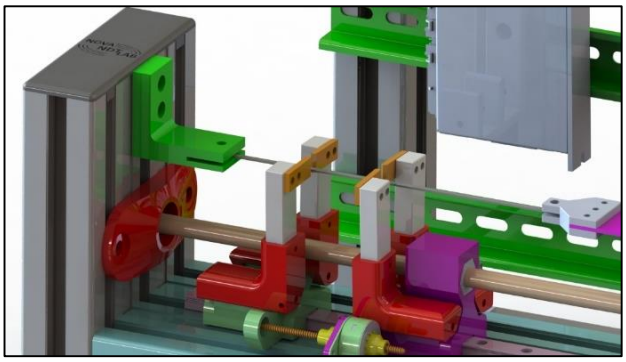

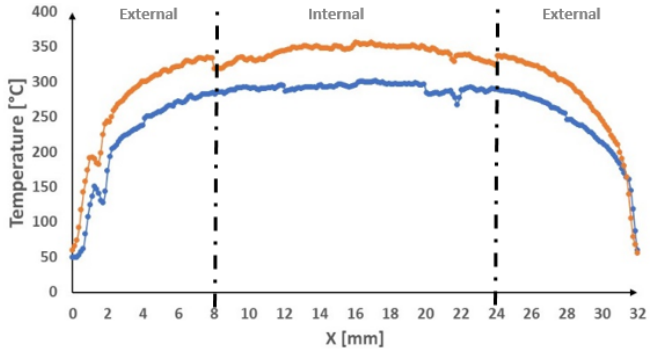
External
Internal
External
Temperature [°C]
X [mm]

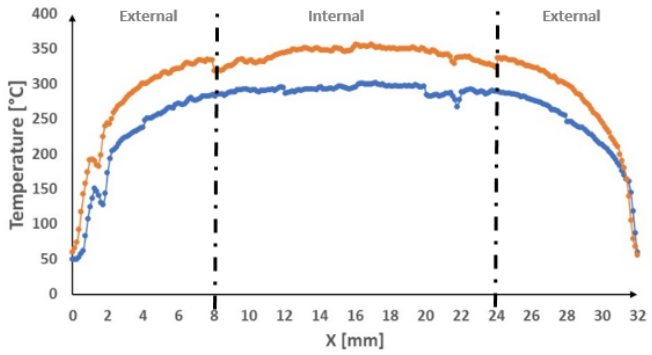
External
Internal
External
Temperature [°C]
X [mm]

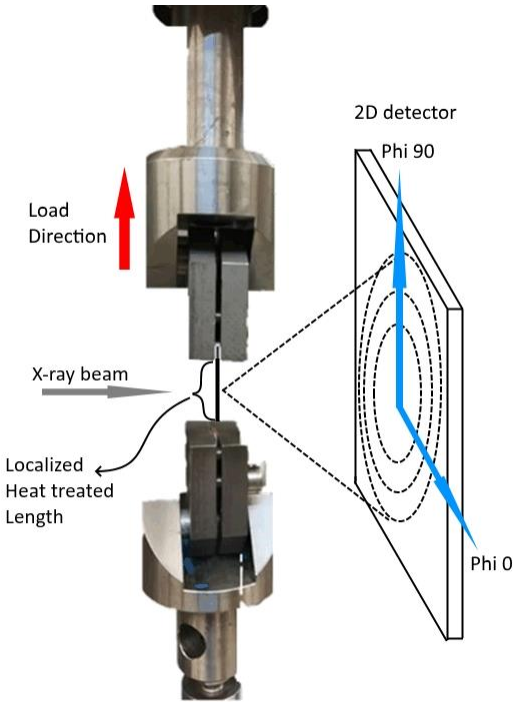
2D detector
Phi 90
Load
Direction
X-ray beam
Localized
Heat treated
Length
Phi 0

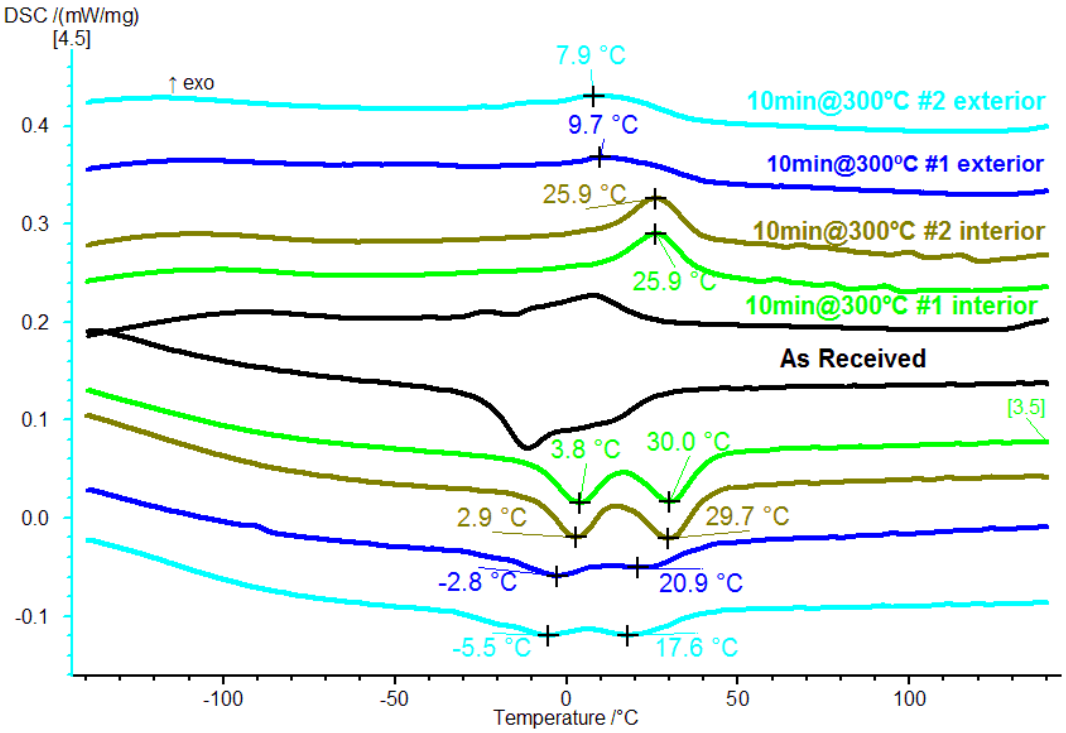
DSC /(mW/mg)
[4.5]
↑ exo
7.9 °C
10min@300°C #2 exterior
9.7 °C
10min@300°C #1 exterior
25.9 °C
10min@300°C #2 interior
25.9 °C
10min@300°C #1 interior
As Received
[3.5]
3.8 °C
30.0 °C
2.9 °C
29.7 °C
-2.8 °C
20.9 °C
-5.5 °C
17.6 °C
0.4
0.3
0.2
0.1
0.0
-0.1
-100
-50
0
50
100
Temperature /°C

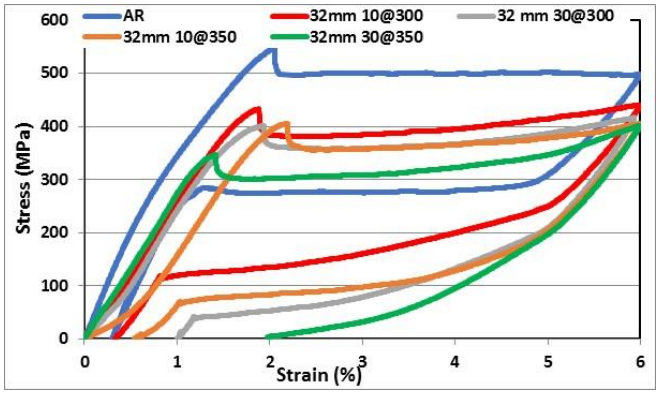
AR
32mm 10@300
32 mm 30@300
32mm 10@350
32mm 30@350
Stress (MPa)
Strain (%)
600
500
400
300
200
100
0
0
1
2
3
4
5
6

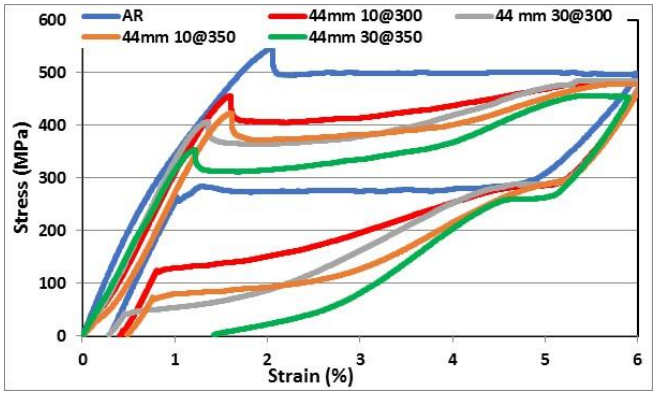
AR
44mm 10@300
44 mm 30@300
44mm 10@350
44mm 30@350
Stress (MPa)
Strain (%)
600
500
400
300
200
100
0
0
1
2
3
4
5
6

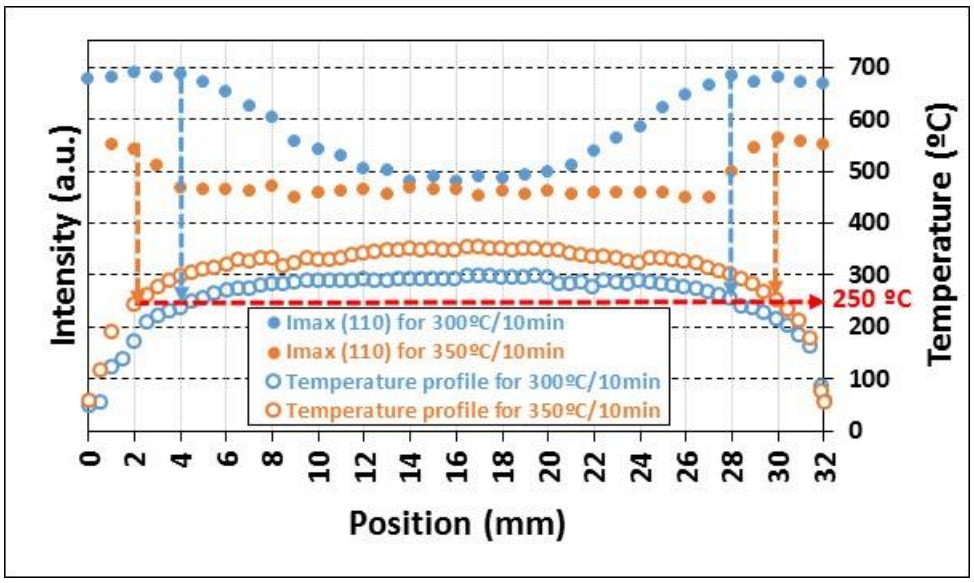
Intensity (a.u.)
Temperature (ºC)
Position (mm)
250 ºC
Imax (110) for 300ºC/10min
Imax (110) for 350ºC/10min
Temperature profile for 300ºC/10min
Temperature profile for 350ºC/10min

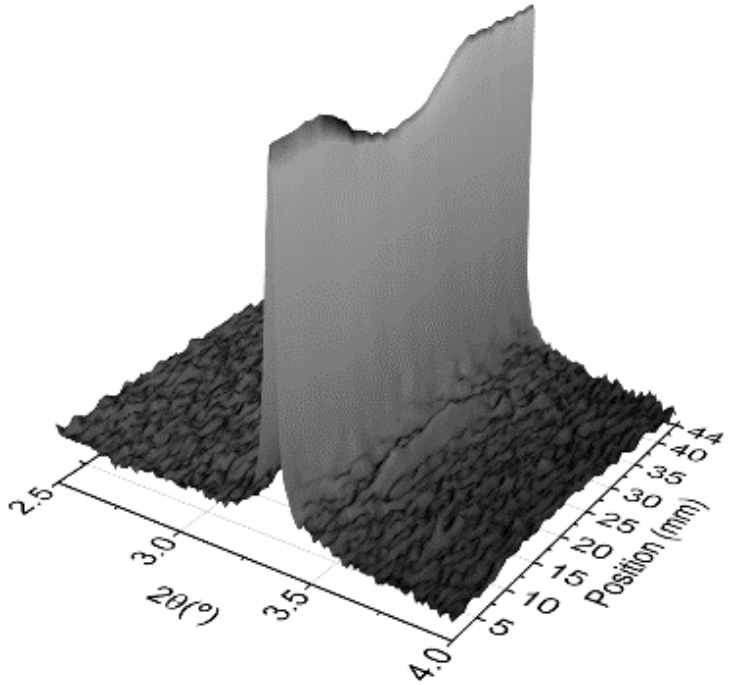
2θ(°)
Position (mm)

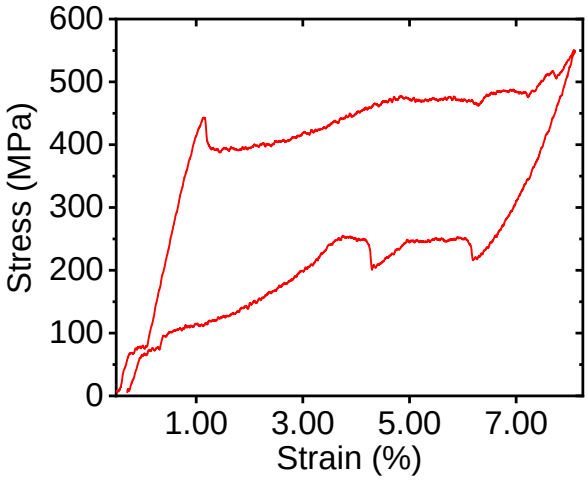
Stress (MPa)
Strain (%)

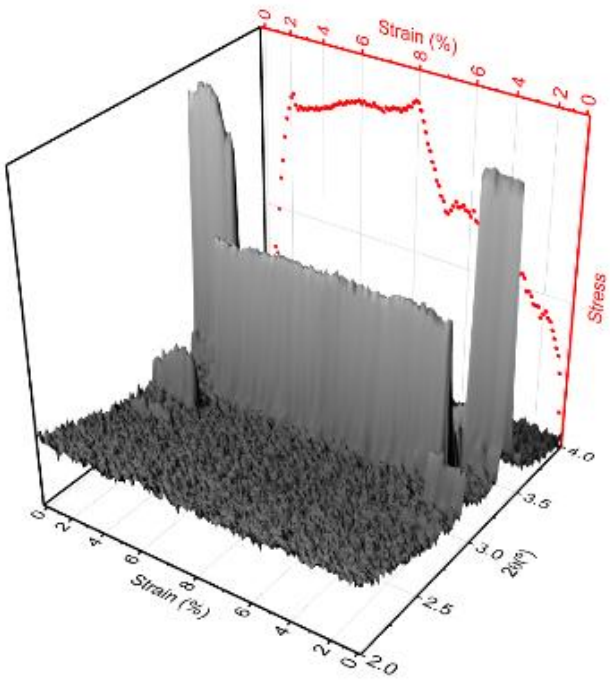
Strain (%)
Stress
Strain (%)
2θ(°)

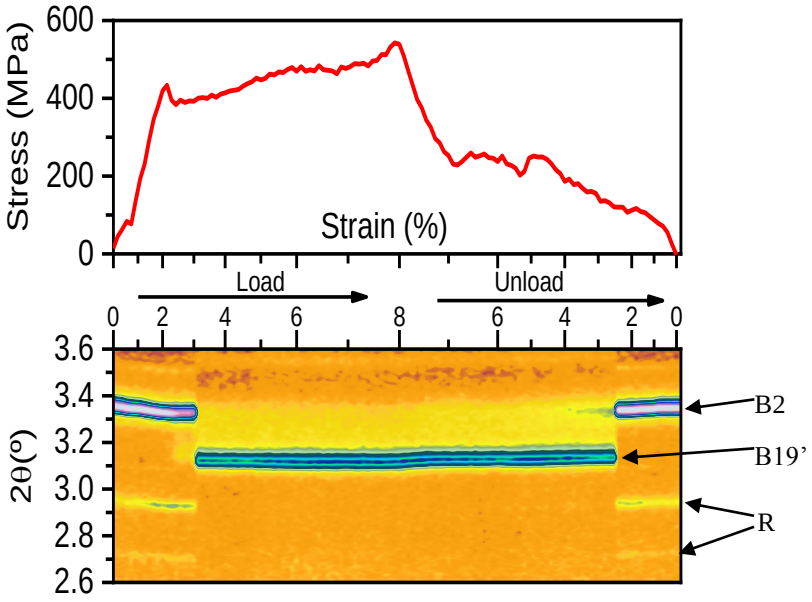
Stress (MPa)
Strain (%)
Load
Unload
2θ(°)
B2
B19'
R

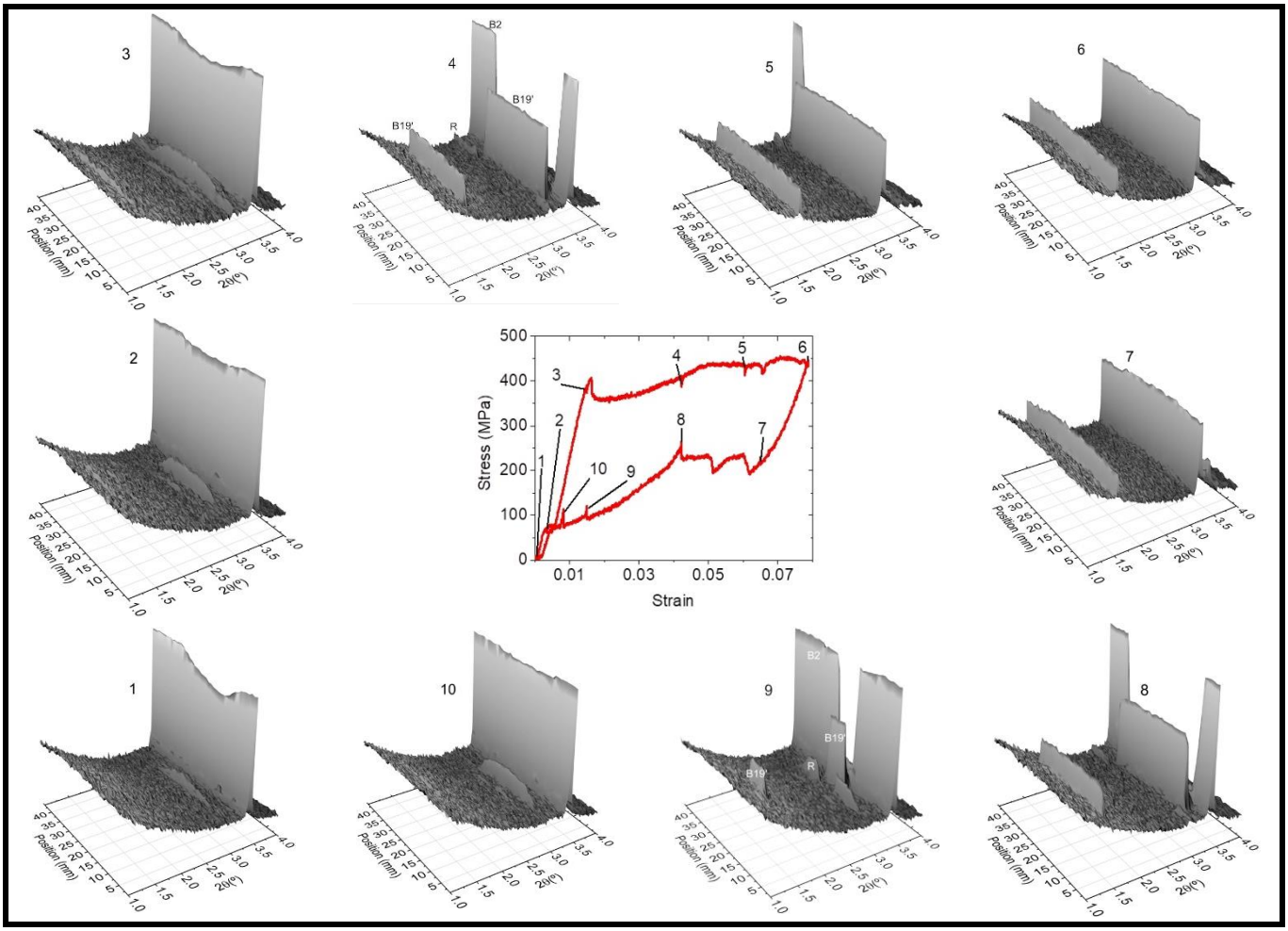
3
4
B2
B19'
B19'
R
5
6
2
Stress (MPa)
Strain
1
2
3
4
5
6
7
8
9
10
7
1
10
9
B2
B19'
B19'
R
8
Position (mm)
2θ(°)

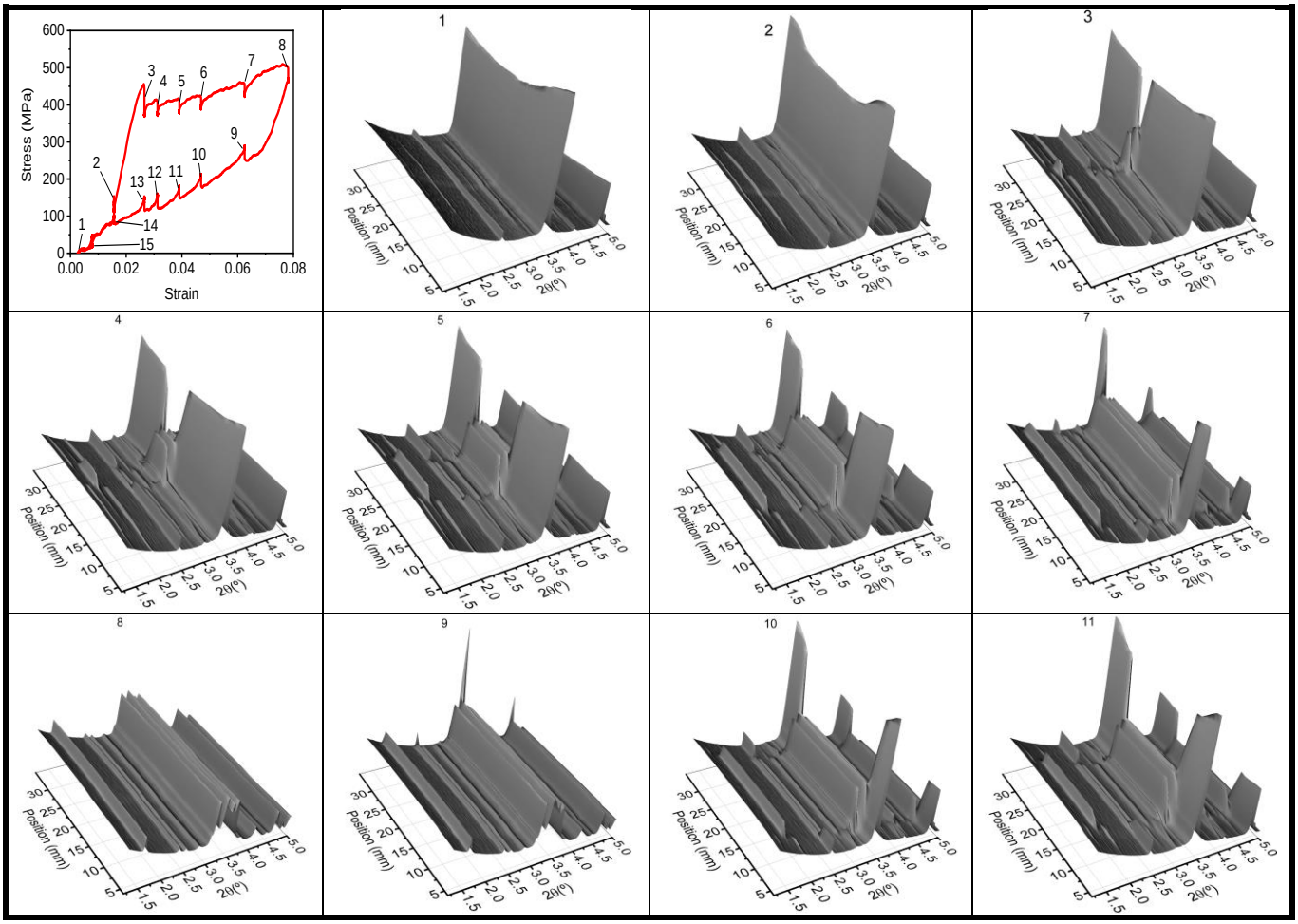
Stress (MPa)
Strain
1
2
3
4
5
6
7
8
9
10
11
12
13
14
15
Position (mm)
2θ(°)